

Abundance analysis of cool extreme helium star: LSS 3378

Gajendra Pandey and Bacham E. Reddy¹

Indian Institute of Astrophysics, Bangalore 560034, India

¹ *Visiting Observer, Cerro-Tololo Inter-American Observatory*

Accepted . Received ; in original form 2006

ABSTRACT

Abundance analysis of the cool extreme helium (EHe) star LSS 3378 is presented. The abundance analysis is done using LTE line formation and LTE model atmospheres constructed for EHe stars.

The atmosphere of LSS 3378 shows evidence of H-burning, He-burning, and *s*-process nucleosynthesis. The derived abundances of iron-peak and α -elements indicate absence of selective fractionation or any other processes that can distort chemical composition of these elements. Hence, the Fe abundance ($\log \epsilon(\text{Fe}) = 6.1$) is adopted as an initial metallicity indicator. The measured abundances of LSS 3378 are compared with those of R Coronae Borealis (RCB) stars and with rest of the EHe stars as a group.

Key words: stars: abundances – stars: AGB and post-AGB – stars: chemically peculiar – stars: evolution.

1 INTRODUCTION

The extreme helium stars (EHes) are supergiants with peculiar chemical composition. The atmospheres of these supergiants with effective temperature in the range 8000 – 35000 K are devoid of hydrogen, and are enriched with helium, carbon, and nitrogen with respect to the atmospheres of normal main-sequence stars. Helium is the most abundant element in their atmospheres. There are about 21 known EHes. There are 5 cool EHes, stars with effective temperatures 8000 to 13000 K, of which 4 were analysed by Pandey et al. (2001). The remaining one cool EHe LSS 3378 is analysed here.

Star No. 3378 (LSS 3378) in the catalog of Stephenson and Sanduleak (1971) was first identified as helium-rich B-type by Drilling (1973). Drilling noticed the absence of Balmer absorption lines, presence of strong He I absorption lines, and the presence of C II line at 4267Å in the spectrum of LSS 3378. Drilling also noted strong Mg II line at 4481Å and Si II lines in absorption indicating a spectral class of about B8 but, however, suggested somewhat earlier class than this because of the presence of several weak O II lines. Jeffery et al. (2001) reported the effective temperature of LSS 3378 to be about 10500 K by fixing E_{B-V} using *IUE* data and *UBV* photometry. However, Jeffery et al. also reported that the *IUE* data for this star are very noisy. Drilling et al. (1984) were the first to derive an effective temperature for LSS 3378, obtaining $9400 \pm 500\text{K}$, using the same procedure adopted by Jeffery et al.

R Coronae Borealis (RCB) stars, which are hydrogen-deficient F- and G-type supergiants, overlap in their effective

temperatures with cooler EHes. With this abundance analysis of LSS 3378, we have the chemical composition of all the 5 known cool EHes which are closely related to RCB stars. Our abundance analysis is based on the high resolution optical spectrum.

2 OBSERVATIONS

The spectrum of LSS 3378 was obtained on 2002 June 19 with the 4-m Blanco telescope and the Cassegrain echelle spectrograph at CTIO in Chile. Three exposures of 25 minutes each, spectra covering the wavelength interval 5000 – 8200Å without gaps, were recorded at a resolving power of $R = 30,000$. The Image Reduction and Analysis Facility (IRAF) software packages were used to reduce the recorded spectra. The Th-Ar hollow cathode lamp provided lines for wavelength calibration. A final spectrum was obtained by co-adding these three individual wavelength calibrated spectra from the three exposures. The maximum signal-to-noise (S/N) in the continuum (per pixel) of the co-added spectrum is between 200 and 250 at the middle of each echelle order.

The Na D lines in the spectrum of LSS 3378 are very strong and appear to be saturated as seen in the spectra of other cool EHes: FQ Aqr, LS IV –14°109, BD –1°3438, and LS IV –1°2. These saturated Na D lines in the spectra of cool EHes are certainly interstellar in origin. The Na D lines in the spectra of cool EHes are stronger than in any other spectrum of normal star. Note that, lines of ionized metals

arXiv:astro-ph/0604023v1 3 Apr 2006

of the iron group are plentiful in the cool EHe’s spectrum. These lines are much stronger when compared with those observed in early A-type and late B-type normal stars. This notable feature of the spectra of cool EHe’s is attributable to the lower opacity in the atmosphere due to hydrogen deficiency.

3 ABUNDANCE ANALYSIS - METHOD

3.1 Procedure

For the abundance analysis of LSS 3378, same procedure is followed as described in Pandey et al. (2001, 2004, 2006). The analysis uses line-blanketed hydrogen-deficient model atmospheres computed by the code STERNE (Jeffery, Woolf & Pollacco 2001). STERNE model atmosphere was combined with the Armagh LTE code SPECTRUM (Jeffery, Woolf & Pollacco 2001) to compute the equivalent width of a line or a synthetic spectrum. In matching a synthetic spectrum to an observed spectrum we include broadening due to the instrumental profile, the microturbulent velocity ξ and assign all additional broadening, if any, to rotational broadening. We use the standard rotational broadening function $V(v \sin i, \beta)$ with the limb darkening coefficient set at $\beta = 1.5$ (Jeffery, Woolf & Pollacco 2001). Observed unblended line profiles are used to obtain the projected rotational velocity $v \sin i$. Synthetic line profile, including the broadening due to instrumental profile, for the adopted model atmosphere ($T_{\text{eff}}, \log g, \xi$) and the abundance, is found to be sharper than the observed. This extra broadening in the observed profile is attributed to rotational broadening.

The adopted gf -values for C, N, O, are from Wiese, Fuhr & Deters (1996), and for rest of the elements are from NIST database^{*}, Kurucz’s database[†], Thévenin (1989, 1990), and the compilations by R. E. Luck (private communication). The Stark broadening and radiative broadening coefficients, if available, are mostly taken from the Kurucz’s database. The data for computing He I profiles are the same as in Jeffery, Woolf & Pollacco (2001). Table A1 has the detailed line list used in our analysis.

3.2 Atmospheric parameters

The model atmospheres are defined by the effective temperature, the surface gravity, and the chemical composition. The input composition of He and C (the C/He ratio) is fully consistent with the C/He ratio derived from the observed spectrum with that model; He and C abundances, particularly He, dominate the continuous opacity. The input composition of rest of the elements is solar with H/He fixed at 10^{-4} by number.

The analysis involves the determination of effective temperature (T_{eff}), surface gravity ($\log g$), and microturbulent velocity (ξ) before estimating the photospheric elemental abundances of the star. These parameters are determined from the line spectrum. The microturbulent velocity ξ (in km s^{-1}) is first determined by the requirement that the

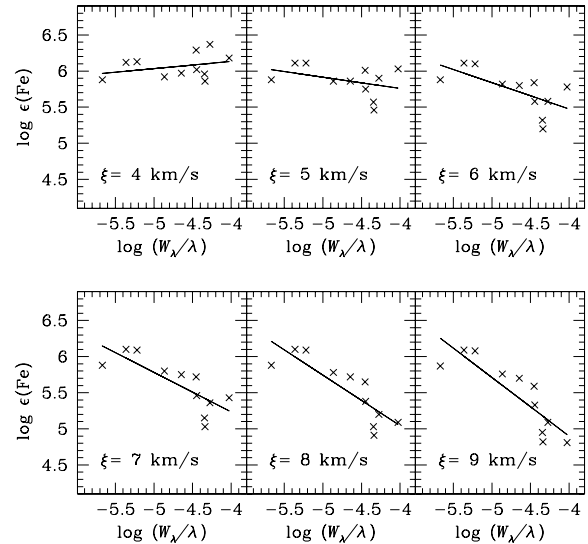


Figure 1. Abundances from Fe II lines for LSS 3378 versus their reduced equivalent widths ($\log W_{\lambda}/\lambda$). A microturbulent velocity of $\xi \simeq 4.5 \text{ km s}^{-1}$ is obtained from this figure.

abundance from a set of lines of the same ion with similar excitation potentials be independent of a line’s equivalent width. For an element represented in the spectrum by two or more ions, imposition of ionization equilibrium (i.e., the same abundance is required from lines of different stages of ionization) defines a locus in the ($T_{\text{eff}}, \log g$) plane. Different pairs of ions of a common element provide loci of very similar slope in the ($T_{\text{eff}}, \log g$) plane.

An indicator yielding a locus with a contrasting slope in the ($T_{\text{eff}}, \log g$) plane is required to break the degeneracy presented by ionization equilibria. A potential indicator is a He I line. For stars hotter than about 10,000 K, the He I lines are less sensitive to T_{eff} than to $\log g$ on account of pressure broadening due to the quadratic Stark effect. The diffuse series lines are, in particular, useful because they are less sensitive to the microturbulent velocity than the sharp lines. A second indicator may be available: species represented by lines spanning a range in excitation potential may serve as a thermometer measuring T_{eff} with a weak dependence on $\log g$.

4 LSS 3378 - ABUNDANCE ANALYSIS RESULTS

First to determine is the microturbulent velocity ξ . We adopt a model atmosphere with $T_{\text{eff}} = 10000 \text{ K}$, which is close to that found by Jeffery et al. (2001), and adopt $\log g = 1.0$ which is a fair assumption for these hydrogen-deficient supergiants. ξ is found to be 4.5 and 7.5 km s^{-1} from Fe II and C I lines, respectively. We adopt $\xi = 6 \text{ km s}^{-1}$ for abundance determination, and Figure 1 illustrates the method for obtaining ξ . Fe II lines used for determining ξ were of similar lower excitation potential and so was the case for C I lines.

The T_{eff} was estimated from Fe II lines spanning excitation potentials from 3 eV to 11 eV. For $\xi = 4.5 \text{ km s}^{-1}$,

^{*} http://physics.nist.gov/PhysRefData/ASD/lines_form.html

[†] <http://kurucz.harvard.edu>

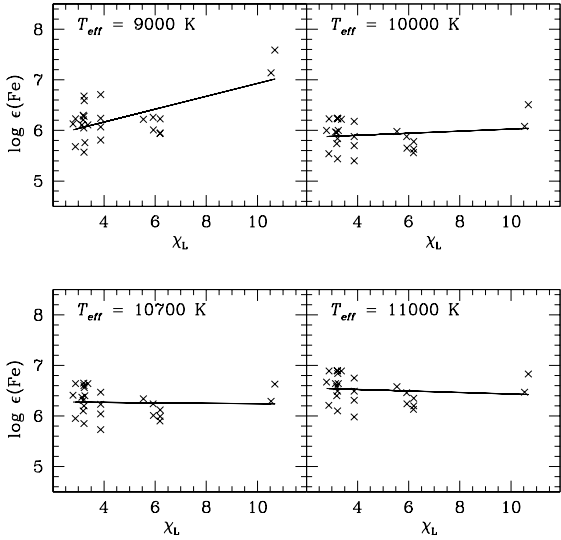


Figure 2. Excitation equilibrium for LSS 3378 using Fe II lines, and models with $\log g = 0.5$.

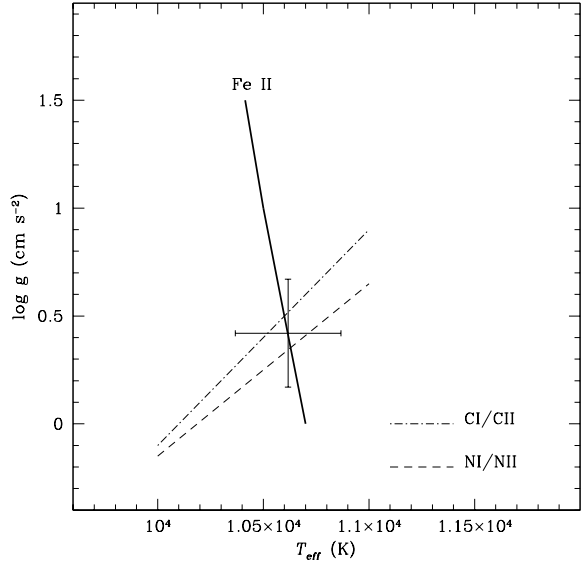


Figure 3. The T_{eff} vs $\log g$ plane for LSS 3378. Loci satisfying ionization equilibria are plotted – see key on the figure. The locus satisfying the excitation balance of Fe II lines is shown by thick solid line. The cross shows the adopted model atmosphere parameters.

models (T_{eff} , $\log g$) were found which gave the same abundance independent of excitation potential. The T_{eff} determined from Fe II lines somewhat depends on the adopted surface gravity. Figure 2 illustrates the method for obtaining T_{eff} . Ionization equilibrium loci for C I/C II and N I/N II are shown in Figure 3. These with the T_{eff} determined from the excitation equilibrium of Fe II lines, which is a function of surface gravity, gives the estimate of the stellar parameters: $T_{\text{eff}} = 10600 \pm 250$ K, $\log g = 0.4 \pm 0.25$ cgs, and $\xi = 6 \pm 2$

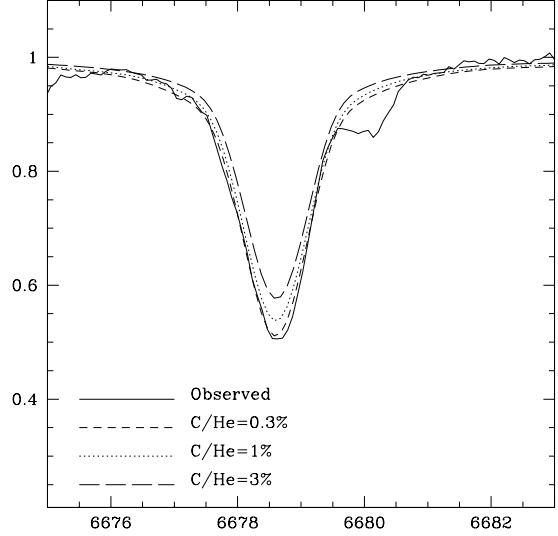


Figure 4. LSS 3378’s observed and synthesized He I line profile at 6678.15 Å. The He I line profiles are synthesized using the model $T_{\text{eff}} = 10600$ K and $\log g = 0.4$, for different values of C/He – see key on the figure.

km s⁻¹ (Figure 3). Thus, the abundance analysis was conducted for the model atmosphere (10600, 0.4, 6.0). At this T_{eff} which is close to 11000 K, electron scattering (most of the free electrons from photoionization of neutral helium), and photoionization of neutral helium are the major sources of continuum opacity in the line forming regions (Pandey et al. 2001). Hence, for LSS 3378 it is evident that helium controls the continuum opacity, and the C/He ratio is directly determined from the measured equivalent widths of C I and C II lines observed in the spectrum of LSS 3378. The C I lines give $\log \epsilon(\text{C}) = 9.53 \pm 0.19$. Four C II lines give 9.44 ± 0.11 . The abundances from C I and C II lines are in good agreement, and imply a C/He = 1%. At the T_{eff} of LSS 3378, the He I lines are mildly sensitive to the C/He ratio. The C/He ratio may be derived by fitting the He I lines at 5048, 5876, and 6678 Å (Figure 4); the blending Ne I line at 6678 Å is taken into account. These He I lines give C/He = $0.8 \pm 0.1\%$, where the uncertainty reflects only the scatter of the three results. LSS 3378’s final abundances, for key elements, derived for C/He = 1% are summarized in Table 1; also given are solar abundances from Table 2 of Lodders (2003) for comparison. The individual elemental abundances listed in Table 1 are given as $\log \epsilon(i)$, normalized such that $\log \sum \mu_i \epsilon(i) = 12.15$ where μ_i is the atomic weight of element i . The lines used for abundance analysis including the mean abundance, and the line-to-line scatter are given in Table A1. The abundance errors due to the uncertainty in the adopted stellar parameters are given in Table 2. The deduced $v \sin i$ is about 26 km s⁻¹.

5 ABUNDANCES

The derived abundances of the EHe LSS 3378 are compared with the measured abundances, taken from the literature, of

Table 1. Adopted key elemental abundances for LSS 3378

Star	H	He	C	N	O	Mg	Al	Si	P	S	Ti	Cr	Mn	Fe	Y	Zr	Ba
LSS 3378	7.18	11.50	9.46	8.26	9.29	5.97	5.98	6.62	4.85	6.52	4.29	4.47	4.57	6.11	2.85	3.51	2.49
Sun	12.00	10.98	8.46	7.90	8.76	7.62	6.54	7.61	5.54	7.26	5.00	5.72	5.58	7.54	2.28	2.67	2.25

the other EHes (see Pandey et al. 2006). The photospheric composition of LSS 3378 reveals that the surface material is contaminated by the products of H-burning, and He-burning reactions, as observed for most of the EHes.

LSS 3378’s abundance ratios: Cr/Fe, Mn/Fe, S/Fe, Si/Fe, and Ti/Fe, are as expected for that in metal-poor normal and unevolved stars except for the low Mg/Fe ratio. The abundances of Fe, Cr, and Mn—the iron peak elements, and S, Si, and Ti—the α -elements represent the initial metallicity of LSS 3378 as these elements are expected to be unaffected by H- and the He-burning, and attendant nuclear reactions. We choose Fe to be the indicator of the initial metallicity in LSS 3378 for spectroscopic convenience.

LSS 3378’s derived elemental abundances that are affected by evolution are of H, C, N, O, Ne, Y, Zr, and Ba. Note that, the Ne abundances from Ne I lines are affected by departures from LTE, hence, not discussed here. However, the neon LTE abundances from Ne I lines are listed in Table A1.

Hydrogen—H abundance $\log \epsilon(\text{H})$ is about 7.2 that fits the suggested trend of increasing H with increasing T_{eff} for all the EHes with C/He ratio of about 1%, the exception being the hottest EHe LS IV +6^o2 (see Pandey et al. 2006).

Carbon—The C/He ratio is 0.0083, the mean C/He ratio from 15 EHes, that excludes the two EHes HD 144941 and V652 Her with much lower C/He ratio, is 0.0066.

Nitrogen—Nitrogen is enriched above its initial abundance expected based on the Fe abundance. The observed N abundance is the result of complete conversion of the initial C, N, and O to N via H-burning CN-cycle and the ON-cycles.

Oxygen—Oxygen abundance relative to Fe is overabundant by about 1.5 dex. LSS 3378 fits to the oxygen-rich group of EHes (see Pandey et al. 2006).

Yttrium, Zr, and Ba—Relative to iron, Y, Zr, and Ba are overabundant with respect to solar by about a factor of 80 (1.9 dex), 150 (2.2 dex), and 40 (1.6 dex), respectively. Note that, the measured abundances are based on one or two lines. The observed Y, Zr, and Ba overabundances are attributed to contamination of the atmosphere by *s*-process products.

6 CONCLUSIONS

The abundances of the cool EHe star LSS 3378 are measured. The measured C/He ratio is about 1% similar to most of the EHes. LSS 3378 fits the oxygen-rich group of EHes discussed by Pandey et al. (2006). The measured abundances of Y, Zr, and Ba suggest that in the EHe star LSS 3378, *s*-process nucleosynthesis did occur in its earlier evolution. With this analysis, a total of four EHes: LSS 3378, PV Tel, V1920 Cyg, and LSE 78, show a strong enhancement of Y

Table 2. Abundance errors due to uncertainties in the stellar parameters: ΔT_{eff} , $\Delta \log g$, and $\Delta \xi$. The abundance error due to ΔT_{eff} is the difference in abundances derived from the adopted model (T_{eff} , $\log g$, ξ) and a model ($T_{\text{eff}} + \Delta T_{\text{eff}}$, $\log g$, ξ). The abundance error due to $\Delta \log g$ is the difference in abundances derived from the adopted model (T_{eff} , $\log g$, ξ) and a model (T_{eff} , $\log g + \Delta \log g$, ξ). The abundance error due to $\Delta \xi$ is the difference in abundances derived from the adopted model (T_{eff} , $\log g$, ξ) and a model (T_{eff} , $\log g$, $\xi + \Delta \xi$).

Species	$\Delta T_{\text{eff}} = +300$ [K]	$\Delta \log g = +0.25$ [cgs]	$\Delta \xi = +2.0$ [km s ⁻¹]
H I	-0.19	+0.22	+0.09
C I	-0.18	+0.18	+0.11
C II	+0.02	+0.02	+0.13
N I	-0.18	+0.18	+0.12
N II	+0.04	-0.02	+0.09
O I	-0.17	+0.20	+0.24
Ne I	-0.04	+0.11	+0.41
Na I	-0.17	+0.17	+0.09
Mg II	-0.22	+0.18	+0.28
Al II	-0.12	+0.11	+0.17
Al III	+0.04	-0.05	+0.09
Si II	-0.15	+0.16	+0.26
P II	-0.07	+0.03	+0.05
S II	0.00	+0.18	+0.20
Ti II	-0.27	+0.18	+0.03
Cr II	-0.35	+0.17	-0.05
Mn II	-0.22	+0.17	+0.03
Fe II	-0.25	+0.15	+0.11
Y II	-0.27	+0.19	+0.01
Zr II	-0.28	+0.19	-0.01
Ba II	-0.25	+0.19	+0.01

and Zr attributable to an *s*-process (Pandey et al. 2004, 2006).

An interesting similarity is suggested by the *s*-process abundances in LSS 3378 and those of the RCB stars. The light *s*-process elements are more enhanced than the heavy *s*-process elements in RCB stars (Asplund et al. 2000; Rao & Lambert 2003; Vanture, Zucker, & Wallerstein 1999; Bond, Luck, & Newman 1979). Similar enhancement of light *s*-process elements (Y, Zr) over heavy *s*-process element (Ba) is observed in LSS 3378.

Enrichment of *s*-process elements is not expected for the EHes resulting from a merger of a He with a C-O white dwarf as discussed by Pandey et al. (2004, 2006). However, synthesis by neutrons via the *s*-process may occur during the merger and needs to be explored.

To further improve the chemical analysis, non-LTE calculations should be performed for key elements like N, O, Ne, Si, S, and Fe, and in particular neon.

The observations presented here were obtained at CTIO, National Optical Astronomy Observatories (NOAO),

which is operated by the Association of Universities for Research in Astronomy Inc. (AURA) under a cooperative agreement with the National Science Foundation, USA. We thank the referee Tony Lynas-Gray for drawing our attention to the strong Na D profiles in LSS 3378's spectrum.

REFERENCES

- Asplund, M., Gustafsson, B., Lambert, D. L., Rao, N. K., 2000, *A&A*, 353, 287
 Bond, H. E., Luck, R. E., Newman, M. J., 1979, *ApJ*, 233, 205
 Drilling, J. S., 1973, *ApJ*, 179, L31
 Drilling, J. S., Schönberner, D., Heber, U., Lynas-Gray, A. E., 1984, *ApJ*, 278, 224
 Jeffery, C. S., Starling, R. L. C., Hill, P. W., Pollacco, D. L., 2001, *MNRAS*, 321, 111
 Jeffery, C. S., Woolf, V. M., Pollacco, D. L., 2001, *A&A*, 376, 497
 Pandey, G., Rao, N. K., Lambert, D. L., Jeffery, C. S., Asplund, M., 2001, *MNRAS*, 324, 937
 Pandey, G., Lambert, D. L., Rao, N. K., Jeffery, C. S., 2004, *ApJ*, 602, L113
 Pandey, G., Lambert, D. L., Jeffery, C. S., Rao, N. K., 2006, *ApJ*, 638, 454
 Rao, N. K., Lambert, D. L., 2003, *PASP*, 115, 1304
 Stephenson, C. B., Sanduleak, N., 1971, *Publ. Warner & Swasey Obs.*, 1, 1
 Thévenin, F., 1989, *A&AS*, 77, 137
 Thévenin, F., 1990, *A&AS*, 82, 179
 Vanture, A. D., Zucker, D., Wallerstein, G., 1999, *ApJ*, 514, 932
 Wiese, W. L., Fuhr, J. R., Deters, T. M., 1996, *J. Phys. Chem. Ref. Data*, Monograph No. 7

APPENDIX A: LINES USED FOR ABUNDANCE ANALYSIS

The lines used for the abundance analysis of LSS 3378 are given in Table A1. The lower excitation potential (χ_L), gf -value, measured equivalent width (W_λ) and the abundance ($\log \epsilon$) derived for each line is also listed. The abundances are derived using $C/He = 1.0\%$ model for LSS 3378.

Table A1. Lines used to derive elemental abundances for LSS 3378

Ion	λ (Å)	χ (eV)	$\log gf$	W_λ (mÅ)	$\log \epsilon^a$	Ref. ^b
HI						
	6562.8	10.20	0.71	599	7.18	Jeffery
He I						
	5047.74	21.22	-1.60	Synth ^c	11.54	Jeffery
	5875.62	20.96	0.74	Synth	11.54	Jeffery
	6678.15	21.22	0.33	Synth	11.54	Jeffery
CI						
	5052.18	7.69	-1.30	252	9.26	Wiese
	5380.34	7.69	-1.62	193	9.13	Wiese
	5540.76	8.64	-2.40	81	9.59	Wiese
	5817.70	8.85	-2.86	19	9.41	Wiese
	6001.12	8.64	-2.05	164	9.83	Wiese
	6002.98	8.65	-2.16	83	9.37	Wiese
	6010.68	8.64	-1.96	166	9.75	Wiese
	6014.83	8.64	-1.59	215	9.72	Wiese
	6078.39	8.85	-2.27	74	9.51	Wiese
	6113.15	8.85	-2.63	66	9.79	Wiese
	6115.84	8.85	-2.52	85	9.85	Wiese
	6120.81	8.85	-2.40	84	9.72	Wiese
	6413.55	8.77	-2.00	153	9.78	Wiese
	6568.71	9.00	-2.16	93	9.62	Wiese
	6587.61	8.54	-1.00	268	9.43	Wiese
	6591.46	8.85	-2.40	54	9.47	Wiese
	6595.24	8.85	-2.40	35	9.24	Wiese
	6611.35	8.85	-1.85	123	9.47	Wiese
	6671.85	8.85	-1.66	166	9.55	Wiese
	6688.79	8.85	-2.16	95	9.56	Wiese
	6711.32	8.54	-2.70	50	9.57	Wiese
	7108.93	8.64	-1.59	182	9.48	Wiese
	7111.47	8.64	-1.09	252	9.46	Wiese
	7113.18	8.65	-0.77	288	9.38	Wiese
	7476.18	8.77	-1.57	193	9.60	Wiese
	7685.19	8.77	-1.52	182	9.48	Wiese
	7832.64	8.85	-1.82	123	9.43	Wiese
	7860.88	8.85	-1.15	241	9.48	Wiese
Mean:					9.53±0.18	
CII						
	5537.61	19.50	-1.79	42	9.57	Wiese
	5891.60	18.05	-0.44	204	9.34	Wiese
	6578.05	14.45	-0.03	848	9.36	Wiese
	6582.88	14.45	-0.33	728	9.48	Wiese
Mean:					9.44±0.11	

Table A1 – continued

Ion	λ (Å)	χ (eV)	$\log gf$	W_λ (mÅ)	$\log \epsilon^a$	Ref. ^b
N I						
6008.46	11.60	-1.11		75	8.30	Wiese
6644.96	11.76	-0.86		63	8.03	Wiese
7406.22	12.01	-0.74		68	8.08	Wiese
7423.64	10.33	-0.71		237	8.32	Wiese
7442.30	10.33	-0.38		302	8.40	Wiese
Mean:				8.23±0.16		
N II						
5045.10	18.48	-0.41		79	8.37	Wiese
5666.63	18.47	-0.05		86	8.14	Wiese
5679.56	18.48	0.25		118	8.17	Wiese
5686.21	18.47	-0.55		38	8.05	Wiese
5710.77	18.48	-0.52		79	8.55	Wiese
Mean:				8.26±0.20		
O I						
4968.79	10.74	-1.26		233	9.35	Wiese
5330.74	10.74	-0.88		302	9.35	Wiese
5436.86	10.74	-1.40		208	9.25	Wiese
5555.00	10.99	-1.80		149	9.35	Wiese
6158.19	10.74	-0.30		401	9.41	Wiese
7473.24	14.12	-0.37		86	9.00	Wiese
Mean:				9.29±0.15		
Ne I						
5852.49	16.85	-0.46		302	9.21	NIST
5881.90	16.62	-0.75		280	9.20	NIST
6030.00	16.67	-1.04		231	9.08	NIST
6074.34	16.67	-0.48		338	9.43	NIST
6143.06	16.62	0.10		505	9.93	NIST
6163.59	16.72	-0.60		315	9.39	NIST
6217.28	16.62	-0.96		247	9.11	NIST
6266.50	16.72	-0.36		404	9.78	NIST
6334.43	16.62	-0.32		419	9.76	NIST
6382.99	16.67	-0.23		446	9.85	NIST
6402.25	16.62	0.35		584	9.74	NIST
6506.53	16.67	-0.02		485	9.80	NIST
6598.95	16.85	-0.34		357	9.55	NIST
7032.41	16.62	-0.25		449	9.84	NIST
Mean:				9.55±0.30		
Na I						
5682.63	2.10	-0.70		32	6.40	NIST
6160.75	2.10	-1.23		29	6.89	NIST
8194.82	2.10	0.51		257	6.78	NIST
Mean:				6.69±0.26		
Mg II						
7877.05	10.00	0.39		246	5.89	NIST
7896.37	10.00	0.65		310	6.04	NIST
Mean:				5.97±0.11		

Table A1 – continued

Ion	λ (Å)	χ (eV)	$\log gf$	W_λ (mÅ)	$\log \epsilon^a$	Ref. ^b
Al II						
5593.23	13.26	0.41		95	5.19	NIST
6226.13	13.07	0.05		86	5.39	NIST
6231.72	13.07	0.40		171	5.71	NIST
6823.40	13.07	-0.14		102	5.72	NIST
6837.08	13.08	0.08		122	5.66	NIST
7042.05	11.32	0.35		393	6.52	NIST
Mean:				5.70±0.45		
Al III						
5696.47	15.64	0.24		85	6.04	NIST
5722.65	15.64	-0.07		57	6.03	NIST
Mean:				6.04±0.01		
Si II						
5055.98	10.07	0.44		490	6.86	NIST
5957.56	10.07	-0.35		304	6.72	NIST
5978.93	10.07	-0.06		329	6.59	NIST
6829.83	12.88	-0.27		69	6.31	NIST
Mean:				6.62±0.23		
P II						
5499.69	10.80	-0.30		38	4.69	NIST
6024.13	10.76	0.14		111	4.94	NIST
6034.04	10.74	-0.22		71	4.95	NIST
6165.57	10.80	-0.34		45	4.83	NIST
Mean:				4.85±0.12		
S II						
5009.52	13.62	-0.28		169	6.81	NIST
5014.00	14.07	0.10		173	6.70	NIST
5103.29	13.67	-0.11		108	6.11	NIST
5320.70	15.07	0.49		151	6.56	NIST
5428.64	13.58	-0.13		176	6.72	NIST
5473.60	13.58	-0.18		154	6.57	NIST
5555.97	13.62	-0.99		45	6.32	NIST
5606.09	13.73	0.31		194	6.54	NIST
5616.61	13.66	-0.64		88	6.46	NIST
5659.96	13.68	-0.05		170	6.62	NIST
5664.76	13.66	-0.25		111	6.29	NIST
Mean:				6.52±0.21		
Ti II						
5072.28	3.12	-0.75		36.0	4.18	NIST
5188.68	1.58	-1.21		102.0	4.39	NIST
Mean:				4.29±0.15		
Cr II						
5246.77	3.71	-2.48		18.0	4.42	NIST
5313.56	4.07	-1.65		90.0	4.62	NIST
5420.92	3.76	-2.58		20.0	4.37	NIST
Mean:				4.47±0.13		

Table A1 – *continued*

Ion λ (Å)	χ (eV)	$\log gf$	W_λ (mÅ)	$\log \epsilon^a$	Ref. ^b
Mn II					
5297.06	9.86	0.87	47.0	4.67	Kurucz
6122.45	10.18	0.95	57.0	4.85	Kurucz
7415.81	3.71	-2.20	40.0	4.37	Kurucz
7432.30	3.71	-2.50	21.0	4.37	Kurucz
Mean:				4.57±0.24	
Fe II					
4993.36	2.81	-3.65	113.0	6.32	NIST
5169.03	2.89	-0.87	487.0	6.28	NIST
5197.58	3.23	-2.10	235.0	5.77	NIST
5234.63	3.22	-2.05	278.0	6.02	NIST
5247.95	10.53	0.63	121.0	6.14	NIST
5254.93	3.23	-3.00	97.0	5.77	Kurucz
5272.40	5.96	-2.05	82.0	6.18	NIST
5276.00	3.20	-1.96	242.0	5.64	NIST
5284.11	2.89	-3.19	110.0	5.86	NIST
5362.87	3.20	-2.70	192.0	6.03	Kurucz
5525.13	3.27	-4.61	24.0	6.64	Kurucz
5534.85	3.25	-2.93	195.0	6.29	NIST
5591.37	3.27	-4.69	12.0	6.40	Kurucz
5627.50	3.39	-4.36	33.0	6.62	NIST
5952.51	5.96	-2.05	61.0	5.97	Kurucz
5961.71	10.68	0.69	162.0	6.41	Kurucz
5991.38	3.15	-3.74	82.0	6.32	NIST
6147.74	3.89	-2.70	123.0	5.94	Kurucz
6149.26	3.89	-2.92	118.0	6.13	NIST
6175.15	6.22	-2.00	64.0	6.08	Kurucz
6179.38	5.57	-2.81	42.0	6.32	NIST
6247.56	3.89	-2.52	199.0	6.21	NIST
6331.96	6.22	-1.96	48.0	5.87	Kurucz
6446.41	6.22	-2.16	38.0	5.97	NIST
7462.41	3.89	-2.70	90.0	5.68	Kurucz
Mean:				6.11±0.27	
Y II					
5205.73	1.03	-0.34	28.0	2.85	Luck
Zr II					
4962.29	0.97	-1.69	6.0	3.42	Thevenin
5350.09	1.83	-0.93	19.0	3.60	Thevenin
Mean:				3.51±0.13	
Ba II					
6496.90	0.60	-0.37	14.0	2.49	Luck

^aNormalized such that $\log \sum \mu_i \epsilon(i) = 12.15$

^bSources of gf -values

^cSpectrum synthesis

References:

Jeffery	Jeffery, Woolf, & Pollacco (2001)
Kurucz	Kurucz's database
Luck	Compilations by R. E. Luck
NIST	NIST database
Thevenin	Thévenin (1989, 1990)
Wiese	Wiese, Fuhr, & Deters (1996)